FCI-AEKF: A Robust GNSS/5G Hybrid Positioning Framework with Dynamic Motion and Noise Adaptation

JianQing Wang[1], Zhongliang Deng[1,*], Fen Qiu[2], Mingyang Ma[1] and Shan Xu[3]

[1]Beijing University of Posts and Telecommunications (BUPT),10 Xitucheng Road, Haidian district, Beijing, China
[2]Nanchang University Institute of Technology,No.199, Wusi Avenue, Gongqing City, Jiujiang, Jiangxi Province, China
[3]Traffic Management Corps of Jiangxi Provincial Public Security Department,No. 997 Fenghuang North Avenue, Honggutan District, Nanchang City, Jiangxi Province, China

Abstract

This paper presents a Fast Covariance Intersection-based Adaptive Extended Kalman Filter (FCI-AEKF) framework for PPP-RTK and 5G integrated positioning. The framework addresses key challenges in GNSS-5G fusion, including limited use of PPP-RTK's high precision, slow error convergence from simple motion models, and distance-dependent 5G measurement noise. It enables multi-rate fusion of PPP-RTK and 5G data, combining high-rate 5G updates with PPP-RTK corrections. A dynamic motion model switching strategy is proposed to adaptively select between constant velocity (CV) and constant acceleration (CA) models based on real-time vehicle dynamics. Additionally, a distance-based noise model is introduced to adjust measurement noise covariance, enhancing robustness under varying conditions. Experimental results on open-source GNSS data from The Hong Kong Polytechnic University demonstrate that the proposed method outperforms existing GNSS-5G fusion approaches in accuracy, robustness, and resistance to interference.

Keywords

5G-GNSS Integration, FCI-AEKF, Vehicle Motion Prediction, Noise Estimation

1. Introduction

GNSS generally offers accurate positioning but faces severe challenges in dense urban areas and highway interchanges due to signal blockage, multipath, and poor satellite geometry. While fusion with INS, LiDAR, or vision systems can improve performance, these methods often suffer from accumulated drift, high costs, or increased complexity.

Precise Point Positioning (PPP), with ambiguity resolution and atmospheric corrections, achieves centimeter-level accuracy, and its real-time extension PPP-RTK reduces convergence time to approximately 30 seconds. However, PPP-RTK still struggles with limited satellite visibility and non-line-of-sight (NLOS) issues. Meanwhile, 5G technology provides wide coverage, low latency, and dense network infrastructure, enabling sub-meter positioning accuracy and serving as a promising complement to GNSS, particularly in challenging environments [1].

Recent research increasingly focuses on GNSS/5G integrated positioning due to its potential for low-cost, high-precision, and robust localization [2]. Existing methods mainly fall into three categories: (i) theoretical analyses deriving position and velocity error bounds [3]; (ii) point positioning approaches using clustering, particle filters, or tightly coupled nonlinear fusion [4, 5]; and (iii) time-based state estimation via adaptive Kalman filtering [6].

However, several limitations remain. GNSS-based solutions still heavily rely on SPP, leading to significant errors under dynamic conditions. Moreover, many studies restrict 5G measurement rates to 1 Hz, despite the standard supporting much higher positioning rates, limiting their applicability in fast-changing environments.

IPIN-WCAL 2025: Workshop for Computing & Advanced Localization at the Fifteenth International Conference on Indoor Positioning and Indoor Navigation, September 15–18, 2025, Tampere, Finland
*Corresponding author.
wjq666@bupt.edu.cn (J. Wang); dengzhl@bupt.edu.cn (Z. Deng); whl@ncu.edu.cn (F. Qiu); mingyangma@bupt.edu.cn (M. Ma); liufangya@163.com (S. Xu)

To address these gaps, this paper introduces an adaptive model-switching strategy that dynamically selects appropriate motion models based on vehicle dynamics. In addition, a distance-aware noise model and a dynamic fusion weighting mechanism are designed to enable real-time covariance adaptation, enhancing robustness and positioning accuracy under diverse signal conditions.

Fig. 1 illustrates our proposed hybrid positioning system integrating PPP-RTK, 5G PRS, and CORS corrections for urban scenarios.

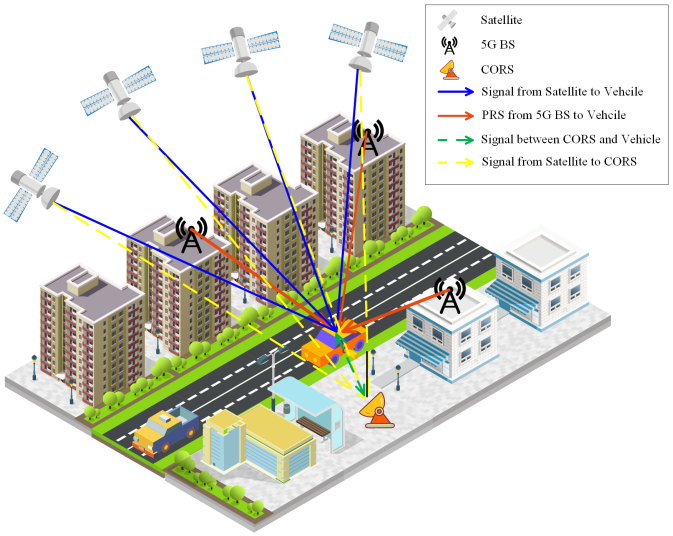

Figure 1: Illustration of the proposed GNSS-5G hybrid positioning framework integrating satellite signals, 5G PRS, and CORS corrections in an urban environment.

To this end, we propose a Fast Covariance Intersection-based Adaptive Extended Kalman Filter (FCI-AEKF) framework, with key contributions:

- First integration of PPP-RTK and 5G in a multi-rate fusion framework, leveraging precise corrections for enhanced accuracy over SPP-based methods.
- An adaptive motion model switching strategy to improve tracking under varying dynamics.
- A distance-based noise model for real-time adjustment of measurement noise covariance, improving robustness.
- A dynamic localization mode-switching strategy to maintain positioning continuity under degraded GNSS/5G conditions.

2. System model

2.1. PPP-RTK Measurement Model

The linearized observation equations for pseudorange and carrier phase of the nth satellite on frequency f are:

$$\Delta P_f^n = e_n \cdot \delta X_n + c \cdot \delta t_{sys} + \alpha^n T_Z + \beta^n I^n - \delta t_f^n + \delta t_{r,f} + \varepsilon_p \tag{1}$$

$$\Delta \Phi_f^n = e_n \cdot \delta X_n + \delta t_{sys} + \alpha^n T_Z - \beta^n I^n + \delta N_f^n + \varepsilon_\phi \tag{2}$$

Here, e_n and δX_n represent the direction cosine and position correction, respectively. c is the speed of light, δt_{sys} is the receiver clock bias, α^n and β^n are mapping functions, and T_Z, I^n denote tropospheric and ionospheric delays. δN_f^n is carrier phase ambiguity, and ε_p, ε_ϕ are Gaussian noise terms. Satellite clock and relativistic effects are assumed corrected [7].

I^n in (1) and (2) can be refined via the DESIGN model:

$$I^n = a_0 + a_1 \delta l + a_2 \delta b + a_3 \delta l^2 + a_4 \delta b^2 + r_r^n + \varepsilon_I \tag{3}$$

where a_i model spatial ionospheric variations, δl and δb are longitudinal and latitudinal differences, r_r^n captures temporal variations, and ε_I is noise.

The pseudorange and carrier phase differences are further expressed as:

$$\Delta P_f^n = P_f^n - \sqrt{(x_n - x_{r,k-1})^2 + (y_n - y_{r,k-1})^2 + (z_n - z_{r,k-1})^2} \tag{4}$$

$$\Delta \Phi_f^n = P_f^n - \sqrt{(x_n - x_{r,k-1})^2 + (y_n - y_{r,k-1})^2 + (z_n - z_{r,k-1})^2} \tag{5}$$

where (x_n, y_n, z_n) and $(x_{r,k-1}, y_{r,k-1}, z_{r,k-1})$ are satellite and receiver positions.

The PPP-RTK state vector is then:

$$x_{PPP-RTK} = \begin{pmatrix} \delta X_n & t_r & \delta t_{sys} & \delta t_{r,f} & N_r^n & a_i r_r^n \end{pmatrix}^T \tag{6}$$

2.2. 5G Measurement Model

The 5G standard defines downlink Positioning Reference Signals (PRS) for DL-TDOA-based multilateration. Base stations broadcast PRS after receiving assistance data, including their locations. The UE cross-correlates the received PRS with a local sequence to estimate arrival times and compute DTDOA. With MIMO antennas, DOA can be estimated using the LAMBDA method.

As signal acquisition is not the focus of this work, technical details are omitted. When the 5G receiver detects k signals at time m, the 5G measurement model is:

$$\mathbf{Z}_{5G}^k[m] = \left[\delta\tau_m, \varphi_m, \theta_m\right]^T = \mathbf{h}_{5G}^k(\mathbf{s}_m) + \mathbf{n}_{5G}^k[m] \tag{7}$$

Here, $\delta\tau_m = \tau_m^k - \tau_m^1$ is the time-difference between base stations k and 1. The angles φ_m and θ_m denote azimuth and elevation, respectively. $\mathbf{n}_{5G}^k[m]$ represents measurement noise.

The state vector at time m is:

$$\mathbf{s}_m = \left[\mathbf{X}_m, \mathbf{V}_m, \mathbf{A}_m, \rho_n, \varphi_n\right]^{\mathrm{T}} \tag{8}$$

where $\mathbf{X}_m$, $\mathbf{V}_m$, and $\mathbf{A}_m$ are the 3D position, velocity, and acceleration, respectively; ρ_n and φ_n denote GNSS clock offset and skew.

The nonlinear 5G measurement function is:

$$\mathbf{h}_{5G}^k(\mathbf{s}_m) = \begin{bmatrix} \dfrac{d_m^k - d_m^1}{c} + \rho_n \\ \arctan\left(\dfrac{\Delta y_m^k}{\Delta x_m^k}\right) \\ \arctan\left(\dfrac{\Delta z_m^k}{\sqrt{(\Delta x_m^k)^2 + (\Delta y_m^k)^2}}\right) \end{bmatrix} \tag{9}$$

where d_m^k is the distance to base station k:

$$d_m^k = \sqrt{(\Delta x_m^k)^2 + (\Delta y_m^k)^2 + (\Delta z_m^k)^2} \tag{10}$$

Given low-cost 5G oscillators, clock drift relative to GNSS must be compensated. The clock offset evolves as:

$$\rho_m = \rho_{m-1} + \varphi_m \Delta t \tag{11}$$

Clock skew follows a first-order autoregressive model:

$$\varphi_m = \eta \cdot \varphi_{m-1} + \varepsilon_m \tag{12}$$

where η is set to 1, and $\varepsilon_m \sim \mathcal{N}(0, \sigma_\varepsilon^2)$ is white Gaussian noise.

3. Proposed Approach

We propose a GNSS-5G hybrid positioning framework leveraging multi-rate fusion, designed to enhance positioning accuracy and robustness. The framework integrates the following core components:

- **Dynamic Motion Model Switching**: An adaptive strategy that switches between constant velocity (CV) and constant acceleration (CA) models based on real-time vehicle dynamics, ensuring accurate state prediction in varying motion conditions.
- **Distance-Dependent Noise Modeling**: A noise adaptation mechanism that adjusts observation noise covariance in the Kalman filter according to the varying distances between the user and 5G base stations, improving the reliability of 5G-based measurements.
- **Fast Covariance Intersection (FCI) Fusion**: An efficient fusion algorithm that combines GNSS and 5G positioning estimates without requiring iterative optimization, ensuring robust performance even under partial observability.

Furthermore, we incorporate a multi-rate mode switching mechanism that dynamically selects the optimal positioning strategy based on the availability and quality of GNSS and 5G signals. This design ensures consistent, reliable performance across complex urban environments.

3.1. Dynamic Motion Model Switching

We propose a Dynamic Motion Model Switching (DMMS) framework that adaptively switches between CV and CA models by analyzing velocity and acceleration. The selection rule is:

$$\text{Model Selection} = \begin{cases} \text{CV Model}, & \dfrac{|\mathbf{V}_m \cdot \mathbf{A}_m|}{\|\mathbf{V}_m\|^2 + \epsilon} < r \\ \text{CA Model}, & \dfrac{|\mathbf{V}_m \cdot \mathbf{A}_m|}{\|\mathbf{V}_m\|^2 + \epsilon} \geq r \end{cases} \tag{13}$$

The system state evolves according to:

$$\mathbf{s}_m = \mathbf{A} \cdot \mathbf{s}_{m-1} + \mathbf{B} + \mathbf{W}_m \tag{14}$$

where $\mathbf{A}$ is selected as either $\mathbf{A}_{\text{CV}}$ or $\mathbf{A}_{\text{CA}}$, depending on the switching rule, and $\mathbf{W}_m$ is Gaussian process noise.

The CV model uses a transition matrix $\mathbf{A}_{\text{CV}}$ that accounts for position, velocity, and clock drift:

$$\mathbf{A}_{\text{CV}} = \begin{bmatrix} \mathbf{I}_{3\times3} & \Delta t \cdot \mathbf{I}_{3\times3} & \mathbf{0} & \mathbf{0} \\ \mathbf{0} & \mathbf{I}_{3\times3} & \mathbf{0} & \mathbf{0} \\ \mathbf{0} & \Delta t^{-1} \cdot \mathbf{I}_{3\times3} & \mathbf{0} & \mathbf{0} \\ \mathbf{0} & \mathbf{0} & \mathbf{0} & \mathbf{A}_k \end{bmatrix}, \quad \mathbf{A}_k = \begin{bmatrix} 1 & \Delta t \\ 0 & \eta \end{bmatrix} \tag{15}$$

Here, $\mathbf{A}_k$ models clock bias as in (11), (12). Acceleration changes do not affect velocity or position updates in this model.

The corresponding process noise covariance matrix $\mathbf{Q}_{\text{CV}}$ is:

$$\mathbf{Q}_{\text{CV}} = \begin{bmatrix} \mathbf{Q}_V & \mathbf{0} & \mathbf{0} \\ \mathbf{0} & \mathbf{U} & \mathbf{0} \\ \mathbf{0} & \mathbf{0} & \mathbf{L} \end{bmatrix} \tag{16}$$

where $\mathbf{Q}_V$, $\mathbf{U}$, and $\mathbf{L}$ are standard formulations capturing process noise.

Similarly, the CA model uses the transition matrix $\mathbf{A}_{\text{CA}}$:

$$\mathbf{A}_{\text{CA}} = \begin{bmatrix} \mathbf{I} & \Delta t \cdot \mathbf{I} & \frac{\Delta t^2}{2} \cdot \mathbf{I} \\ \mathbf{0} & \mathbf{I} & \Delta t \cdot \mathbf{I} \\ \mathbf{0} & \mathbf{0} & \mathbf{I} \end{bmatrix} \tag{17}$$

with the process noise covariance matrix $\mathbf{Q}_{\text{CA}}$ defined as:

$$\mathbf{Q}_{\text{CA}} = \begin{bmatrix} \mathbf{G}\mathbf{U}\mathbf{G}^{\text{T}} & \mathbf{0} \\ \mathbf{0} & \mathbf{L} \end{bmatrix} \tag{18}$$

where $\mathbf{G}$ models higher-order motion effects.

This simplified formulation retains key equations and modeling insights while reducing redundancy. It ensures readability, clarity, and full LaTeX compatibility.

3.2. Dynamic Noise Covariance Modeling

Observation noise is a critical factor affecting positioning accuracy. Traditional EKF methods typically assume fixed noise covariance, which neglects variations caused by changes in sensor-target geometry and environmental conditions. To address this, we incorporate a distance-dependent noise model based on the Cramér–Rao Lower Bound (CRLB), improving the robustness of 5G-based localization.

At time step m, the 5G measurement noise vector $\mathbf{n}_{5G}^{k}[m]$ comprises TDOA and DOA noise components, each modeled as independent zero-mean Gaussian variables:

$$n_{\tau,k1} \sim \mathcal{N}(0, \sigma_{\tau,k1}^2), \quad n_{\varphi,k} \sim \mathcal{N}(0, \sigma_{\varphi,k}^2), \quad n_{\theta,k} \sim \mathcal{N}(0, \sigma_{\theta,k}^2) \tag{19}$$

The CRLBs for TOA and DOA are given by [9, 10, 11, 12]:

$$\sigma_{\tau}^2 = \frac{c^2}{4\pi^2 \cdot t_s \cdot B^3 \cdot \text{SNR}_k}, \quad \sigma_{\varphi,\theta}^2 = \frac{\lambda^2}{8\pi^2 \cdot N_s \cdot AR \cdot \text{SNR}_k} \tag{20}$$

Signal-to-noise ratio (SNR) is modeled using the path loss model [13]:

$$\zeta = \frac{16\pi^2 \cdot d_k^{\alpha_{PL}} \cdot 10^{\beta_{SF}/10}}{\lambda^2} \tag{21}$$

By combining these relationships, we obtain the distance-dependent noise variances for TDOA and DOA:

$$\sigma_{\tau_k}^2 = \sigma_{\tau}^2 \left(\frac{d_k}{d_r}\right)^{\alpha_{PL}}, \quad \sigma_{\varphi_k}^2 = \sigma_{\varphi}^2 \left(\frac{d_k}{d_r}\right)^{\alpha_{PL}}, \quad \sigma_{\theta_k}^2 = \sigma_{\theta}^2 \left(\frac{d_k}{d_r}\right)^{\alpha_{PL}} \tag{22}$$

where $d_r = 1$ is the reference distance.

Thus, the observation noise covariance matrix $\mathbf{R}$ is constructed as:

$$\mathbf{R} = \begin{bmatrix} \mathbf{R}_{\tau} & \mathbf{0} & \mathbf{0} \\ \mathbf{0} & \mathbf{R}_{\varphi} & \mathbf{0} \\ \mathbf{0} & \mathbf{0} & \mathbf{R}_{\theta} \end{bmatrix} \tag{23}$$

This distance-aware model dynamically adjusts measurement noise according to the relative geometry between the user and 5G base stations, enhancing localization reliability and adaptability under varying signal conditions.

3.3. FCI-AEKF-based filtering process

5G systems typically rely on GPS as the primary time synchronization source, with synchronization errors generally within tens of nanoseconds [15]. In real vehicular environments, timing deviations may be negligible, and thus, this work assumes perfect synchronization for simplicity. In our fusion framework, the GNSS and 5G measurements are processed in two stages, each at different sampling rates.

In the first stage of FCI-AEKF, the time index of 5G measurements is defined as:

$$t = T_{m-1} + j, \quad j = 1 : L_r \tag{24}$$

$$T_m = T_{m-1} + L_r \tag{25}$$

where m denotes the GNSS epoch index (starting from 0), and $L_r = \frac{f_{5G}}{f_{sat}}$ represents the ratio of 5G and GNSS sampling rates. This ratio must be an integer.

3.3.1. First Stage of FCI-AEKF

In the first stage, the FCI-AEKF predicts states using 5G TDOA and DOA measurements based on (1), (3), and (4):

$$\mathbf{s}_{5G}^{-}[t] = \mathbf{A} \cdot \mathbf{s}_{5G}^{+}[t-1] + \mathbf{B} \tag{26}$$

$$\mathbf{P}_{5G}^{-}[t] = \mathbf{A}\mathbf{P}_{5G}^{+}[t-1]\mathbf{A}^{\mathrm{T}} + \mathbf{Q}_{5G}[t] \tag{27}$$

Here, $\mathbf{A}$ and $\mathbf{Q}$ depend on the selected motion model. The posterior update follows:

$$\mathbf{K}_{5G}[t] = \mathbf{P}_{5G}^{-}[t]\mathbf{H}_{5G}^{\top}[t]\left(\mathbf{H}_{5G}[t]\mathbf{P}_{5G}^{-}[t]\mathbf{H}_{5G}^{\top}[t] + \mathbf{R}[t]\right)^{-1} \tag{28}$$

$$\mathbf{s}_{5G}^{+}[t] = \mathbf{s}_{5G}^{-}[t] + \mathbf{K}_{5G}[t]\left(\mathbf{Z}_{5G}[t] - \mathbf{h}_{5G}\left(\mathbf{s}_{5G}^{-}[t]\right)\right) \tag{29}$$

$$\mathbf{P}_{5G}^{+}[t] = \left(\mathbf{I} - \mathbf{K}_{5G}[t]\mathbf{H}_{5G}[t]\right)\mathbf{P}_{5G}^{-}[t] \tag{30}$$

where $\mathbf{H}_{5G}[t]$ is the Jacobian matrix of $\mathbf{h}_{5G}$.

3.3.2. Second Step of FCI-AEKF

The second stage uses $\mathbf{s}_{5G}^{+}[t]$ as the reference position $\mathbf{X}_m$ and solves the PPP-RTK state via weighted least squares:

$$\mathbf{s}_{\text{ppp-rtk}}[m] = \left(\mathbf{H}_{\text{sat}}^{T}\mathbf{R}_{\text{sat}}^{-1}\mathbf{H}_{\text{sat}}\right)^{-1}\mathbf{H}_{\text{sat}}^{T}\mathbf{R}_{\text{sat}}^{-1}\mathbf{y}_{\text{sat}}[m] \tag{31}$$

$$\mathbf{P}_{\text{ppp-rtk}}[m] = \left(\mathbf{H}_{\text{sat}}^{T}\mathbf{R}_{\text{sat}}^{-1}\mathbf{H}_{\text{sat}}\right)^{-1} \tag{32}$$

To fuse results, FCI combines the 5G and satellite solutions:

$$\mathbf{P}[m] = \left(w_{5G}[m]\mathbf{P}_{5G}^{-1}[m] + w_{\text{sat}}[m]\mathbf{P}_{\text{sat}}^{-1}[m]\right)^{-1} \tag{33}$$

$$\omega_{5G}[m] = \frac{\|\mathbf{P}_{5G}^{-1}[m] + \mathbf{P}_{\text{sat}}^{-1}[m]\| - \|\mathbf{P}_{\text{sat}}^{-1}[m]\| + \|\mathbf{P}_{5G}^{-1}[m]\|}{2\|\mathbf{P}_{5G}^{-1}[m] + \mathbf{P}_{\text{sat}}^{-1}[m]\|}, \quad \omega_{\text{sat}}[m] = 1 - \omega_{5G}[m] \tag{34}$$

The final fused estimate is:

$$\hat{\mathbf{s}}[m] = \omega_{5G}\mathbf{P}[m]\mathbf{P}_{5G}^{-1}[m]\mathbf{s}_{5G}[m] + \omega_{\text{sat}}\mathbf{P}[m]\mathbf{P}_{\text{sat}}^{-1}[m]\mathbf{s}_{\text{sat}}[m] \tag{35}$$

Here, $\mathbf{s}_{\text{sat}}[m] = \mathbf{X}_m + \delta\mathbf{X}_n$. The fused estimate $\hat{\mathbf{s}}[m]$ is updated at the satellite sampling rate f_{sat}.

3.4. Positioning Mode Switching Strategy

To enhance multi-rate GNSS/5G positioning, we propose a dynamic mode switching strategy that leverages high-rate 5G TDOA/DOA measurements and adapts to variations in GNSS and 5G signal conditions. The system operates in three modes according to signal availability: (i) GNSS/5G fusion mode, where 5G predictions are fused with GNSS updates using FCI-AEKF; (ii) 5G-only mode, activated when fewer than six GNSS satellites are visible; and (iii) PPP-RTK mode, used when fewer than two line-of-sight (LOS) 5G base stations are available. This adaptive mechanism ensures robust and continuous positioning across diverse and challenging environments, maintaining high accuracy even under degraded signal conditions.

The multi-rate switchover scheme for GNSS and 5G hybrid positioning is detailed in Algorithm 1.

Algorithm 1 Multi-rate switchover algorithm for GNSS/5G hybrid positioning

Input: Initial state $s[0]$, GNSS observations, 5G measurements
Output: Fused positioning state $\hat{s}_{sat}^{+}[n]$

1: **for** each GNSS epoch $n = 1$ to N **do**
2: Compute RSRP of all base stations

Estimate path loss from RSRP and transmit power
Identify the two smallest values PL_1, PL_2
Compare PL_1, PL_2 with threshold Th_{PL} to determine N_{LOS}
if $N_{LOS} = 2$ **then**
  Switch to high-rate MRAKF scheme
  for $i = 1$ to R_a **do**
    $t \leftarrow (n-1)R_a + i$
    $\Delta t \leftarrow 1/\mu_{BS}$
    Output posterior estimate $\hat{s}^+_{BS}[t]$
  end for
  Output $\hat{s}^+_{BS}[nR_a]$
  Compute fused state $\hat{s}^+_{sat}[n]$ via Eq. (19)–(21)
else if $N_{LOS} = 1$ **then**
  Switch to centralized EKF
else
  Switch to GNSS SPP
end if
end for
return $\hat{s}^+_{sat}[n]$ =0

3.5. Results and Discussion

3.5.1. Experiment Setup

To evaluate the proposed FCI-AEKF algorithm, a vehicle-based field experiment was conducted around the Haidian campus of Beijing Normal University. A GNSS-5G receiver was mounted on a car, and GNSS measurements were collected at 1 Hz during driving. Distances and angles from simulated 5G base stations to the user equipment (UE) were computed based on ground-truth positions. Synthetic noise was then added to emulate realistic 5G measurement errors. Hybrid positioning was performed by fusing actual GNSS observations with simulated 5G data.

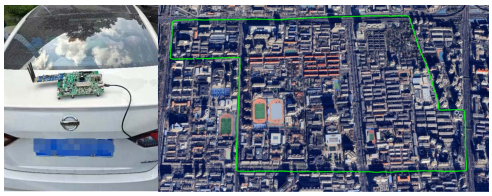

Figure 2: GNSS-5G receiver setup and driving trajectories around the Haidian campus.

3.5.2. Performance Comparison

Fig. 3 shows the positioning error over time for different methods. The proposed FCI-AEKF consistently maintains low error, demonstrating strong stability. In contrast, tcWLS and PPP-RTK exhibit larger error fluctuations and occasional peaks, indicating less robustness under challenging conditions.

Fig. 4 presents the cumulative distribution function (CDF) of positioning errors. The FCI-AEKF achieves the best overall performance, with its CDF curve positioned farthest to the left. TcWLS and PPP-RTK methods yield higher errors, while RAE and AEKF-R provide intermediate performance.

Table 1 summarizes quantitative results. The FCI-AEKF yields the lowest average error (0.31 m) and highest probability of 3D error below 1 m (96.47%). In contrast, PPP-RTK exhibits the largest error and lowest reliability. Other methods, such as RAE and AEKF-R, perform moderately but less consistently than FCI-AEKF.

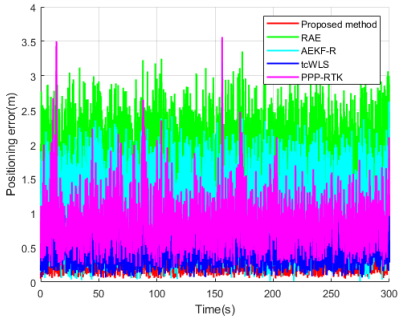

Figure 3: Positioning error over time for FCI-AEKF, RAE, AEKF-R, tcWLS, and PPP-RTK.

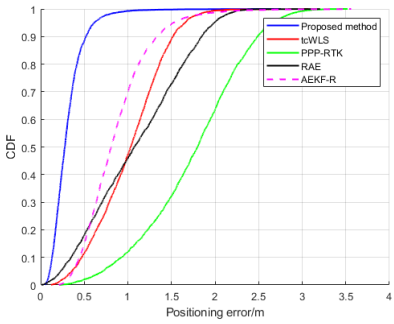

Figure 4: CDF comparison of positioning errors for FCI-AEKF, tcWLS, PPP-RTK, RAE, and AEKF-R.

Table 1
Positioning errors of different methods

Method	5G Rate (samples/s)	Average Error (m)	Probability (3D error < 1m)	Maximum Error (m)
Proposed FCI-AEKF	10	0.31	96.47%	1.74
tcWLS	-	1.21	36.15%	2.52
PPP-RTK	-	1.75	12.36%	3.75
RAE	10	0.51	89.97%	2.33
AEKF-R	10	0.84	69.08%	3.56

3.6. Conclusions

This paper presents the FCI-AEKF framework for GNSS/5G hybrid positioning. By fusing high-rate 5G and GNSS data, the algorithm effectively improves positioning accuracy while maintaining low computational complexity. It also integrates an adaptive motion model switching mechanism and a distance-based noise model to enhance robustness.

Field experiments confirm that FCI-AEKF outperforms conventional GNSS-5G methods, providing lower errors and higher reliability, particularly in challenging environments with limited GNSS visibility.

Overall, the proposed FCI-AEKF demonstrates strong potential for improving positioning performance and system stability in complex real-world scenarios, offering a promising solution for precise GNSS/5G integration.

Acknowledgments

This work was supported by the National Key Research and Development Program of China underGrant No.2022YFB3904700.

Declaration on Generative AI

The authors declare that AI tool was used to assist in improving the language fluency of this paper. All contents, ideas, and conclusions are the authors' own, and the AI tool did not contribute to the scientific results or analysis.

References

[1] H. Wymeersch, G. Seco-Granados, G. Destino, D. Dardari, and F. Tufvesson, "5G mmWave Positioning for Vehicular Networks," *IEEE Wireless Communications*, vol. 24, no. 6, pp. 80–86, Dec. 2017. doi: 10.1109/MWC.2017.1600374.

[2] F. Campolo, A. Blaga, M. Rea, A. Lozano, and X. Costa-Pérez, "5GNSS: Fusion of 5G-NR and GNSS Localization for Enhanced Positioning Accuracy and Reliability," *IEEE Transactions on Vehicular Technology*, vol. 73, no. 9, pp. 13558–13568, Sept. 2024. doi: 10.1109/TVT.2024.3396991.

[3] G. Destino, J. Saloranta, G. Seco-Granados, and H. Wymeersch, "Performance Analysis of Hybrid 5G-GNSS Localization," *2018 52nd Asilomar Conference on Signals, Systems, and Computers*, Pacific Grove, CA, USA, 2018, pp. 8–12. doi: 10.1109/ACSSC.2018.8645207.

[4] W. Zhang, et al., "A GNSS/5G Integrated Three-Dimensional Positioning Scheme Based on D2D Communication," *Remote Sensing*, vol. 14, no. 6, p. 1517, 2022.

[5] J. A. del Peral-Rosado, et al., "Methodology for Simulating 5G and GNSS High-Accuracy Positioning," *Sensors*, vol. 18, no. 10, p. 3220, 2018.

[6] G. Guo, X. Sun, and J. Liu, "5G/GNSS Integrated Vehicle Localization With Adaptive Step Size Kalman Filter," *IEEE Transactions on Vehicular Technology*, vol. 73, no. 11, pp. 16531–16542, Nov. 2024, doi: 10.1109/TVT.2024.3421383.

[7] Q. Zhao, et al., "Refining Ionospheric Delay Modeling for Undifferenced and Uncombined GNSS Data Processing," *Journal of Geodesy*, vol. 93, pp. 545–560, 2019.

[8] M. Goodarzi, D. Cvetkovski, N. Maletic, J. Gutiérrez, and E. Grass, "A Hybrid Bayesian Approach Towards Clock Offset and Skew Estimation in 5G Networks," in *Proc. 2020 IEEE 31st Annual International Symposium on Personal, Indoor and Mobile Radio Communications (PIMRC)*, London, UK, 2020, pp. 1–7, doi: 10.1109/PIMRC48278.2020.9217175.

[9] S. M. Lanzisera and K. Pister, "RF Ranging for Location Awareness," Ph.D. dissertation, *University of California, Berkeley*, 2009.

[10] S. Lanzisera, D. Zats, and K. S. J. Pister, "Radio frequency time-of-flight distance measurement for low-cost wireless sensor localization," *IEEE Sensors Journal*, vol. 11, no. 3, pp. 837–845, Mar. 2011.

[11] I. Peshkov and Y. Nechaev, "Estimation and Minimization of the Cramer-Rao lower bound for radio direction-finding on the azimuth and elevation of planar antenna arrays," *Journal of Communications Software and Systems*, vol. 15, no. 4, pp. 317–328, Dec. 2019.

[12] M. A. Richards, *Fundamentals of Radar Signal Processing*, vol. 1, New York, NY, USA: McGraw-Hill, 2005.

[13] N. T. T. Docomo, "5G Channel Model for Bands up to 100 GHz," Technical Report, 2016.

[14] Committee on Evolution of Untethered Communications, "The Evolution of Untethered Communications," National Academies Press, Washington, DC, USA, 1997.

[15] Z. Wang, *et al.*, "Time Synchronization for 5G and TSN Integrated Networking," *IEEE Journal on Selected Areas in Communications*, 2025.

[16] D. Franken and A. Hupper, "Improved Fast Covariance Intersection for Distributed Data Fusion," *Proc. 7th Int. Conf. on Information Fusion (FUSION)*, vol. 1, pp. 1–8, IEEE, 2005.